bioRxiv preprint doi: https://doi.org/10.1101/2024.11.04.621900; this version posted November 4, 2024. The copyright holder for this preprint (which was not certified by peer review) is the author/funder, who has granted bioRxiv a license to display the preprint in perpetuity. It is made available under aCC-BY-ND 4.0 International license.

Age- and amyloid-β-dependent initiation of neurofibrillary tau tangles: an improved mouse model of Alzheimer's disease without mutations in *MAPT*.

Sneha Desai[1,2], Elena Camporesi[2], Gunnar Brinkmalm[2], Argyro Alatza[3], Jack I. Wood[1,2], Takshashila Tripathi[1], Sumi Bez[4], Nazar Stasyuk[1], Haady B. Hajar[1], Takashi Saito[5], Takaomi C. Saido[6], John Hardy[3,4], Damian M. Cummings[1], Jörg Hanrieder[2,3], Frances A. Edwards[1]

1. Department of Neuroscience, Physiology and Pharmacology, University College London, Gower Street, London, WC1E 6BT, United Kingdom
2. Department of Psychiatry and Neurochemistry, Institute of Neuroscience and Physiology, The Sahlgrenska Academy at the University of Gothenburg, Mölndal, 431 80, Sweden
3. Department of Neurodegenerative Disease, University College London Queen Square Institute of Neurology, London, WC1N 3BG, United Kingdom
4. UK Dementia Research Institute, University College London, Gower Street, London, WC1E 6BT, United Kingdom
5. Department of Neurocognitive Science, Institute of Brain Science, Nagoya City University Graduate School of Medical Sciences, Nagoya, Aichi 467-8601, Japan
6. Laboratory for Proteolytic Neuroscience, RIKEN Center for Brain Science, 2-1 Hirosawa, Wako, Saitama 351-0198, Japan

Abstract

Introducing heterozygous humanized tau to App$^{NL-F/NL-F}$ knock-in mice results in the first mouse model of Alzheimer's disease in which age and amyloid-β pathology interact to initiate neurofibrillary tau tangle pathology, not dependent on mutations in MAPT. Gradual progression from amyloid-β to tau pathology in NLFTau$^{m/h}$ mice opens possibilities for understanding processes precipitating clinical stages of Alzheimer's disease and development of translatable therapies to prevent the onset of tau pathology.

bioRxiv preprint doi: https://doi.org/10.1101/2024.11.04.621900; this version posted November 4, 2024. The copyright holder for this preprint (which was not certified by peer review) is the author/funder, who has granted bioRxiv a license to display the preprint in perpetuity. It is made available under aCC-BY-ND 4.0 International license.

Main text

Much criticism has arisen of mouse models for Alzheimer's disease (AD) due to the limited success in translating therapies to humans, despite promising results in mice. AD is only diagnosed following the development of neurofibrillary tau tangles (NFTs), which occur decades after the accumulation of amyloid-β (Aβ) plaques in the brain[1]. While existing mouse models recapitulating pre-clinical disease stages, in plaque pathology, they only exhibit NFTs if mutations in microtubule-associated protein tau (*MAPT)* are inserted (e.g. 3xTg-AD mice[2]). Such mutations do not occur in AD. The lack of a mouse model that develops NFTs due to rising Aβ poses a significant challenge in studying how plaques drive NFT formation. This hinders efforts to test therapies designed to prevent AD progression to clinical stages. Hence, there is an urgent need to improve existing mouse models by addressing several key factors:

1. Rising Aβ deposition should induce the formation of NFTs, independent of mutations not relevant to AD.
2. A delay should occur between the onset of Aβ plaque accumulation and the development of tau pathology.
3. Development of NFTs must be dependent on old age.

To align the lifelong timecourse of plaque development in sporadic AD, we have developed a model, starting with the $App^{NL\text{-}F/NL\text{-}F}$ (NLF) knock-in mouse[3], which shows a gradual plaque onset from mid-life, progressively increasing through to old age[3,4]. Resistance of amyloid mouse models to forming NFTs could arise from differences between human and mouse in the tau N-terminal region and isoform expression (Fig. S1)[5]. We therefore crossed the NLF mouse with a knock-in humanized *MAPT* mouse[6], such that the *App* mutations were homozygous and the humanized *MAPT* heterozygous ($NLFTau^{m/h}$). This introduces humanized tau, while minimizing potential developmental artefacts that could arise from completely removing murine tau.

Using both western blot and immunoprecipitation combined with liquid-chromatography mass spectrometry (IP-MS), the relative abundance of tau peptides in 24-month-old WT, NLF, $Tau^{m/h}$ and $NLFTau^{m/h}$ was compared. . As expected[7], adult WT and NLF mice lacked the 3 carboxyl-terminal repeat domain (3R) isoforms of tau, whereas $Tau^{m/h}$ and $NLFTau^{m/h}$ exhibited all six isoforms (Fig. 1A). Both methods confirmed that the 3R:4R isoform ratio was similar between $Tau^{m/h}$ and $NLFTau^{m/h}$ mice (Fig. 1B, D) and resembled the approximately equal levels reported in humans, both in healthy controls and AD patients[8]. Other non-phosphorylated tau peptides, in regions analogous between mouse and human tau, were analyzed by IP-MS and found to be unchanged across genotypes (Fig. 1C, Table S1).

Phosphorylated tau (p-tau) residues relevant to human fluid biomarkers[9-11] were analyzed and

bioRxiv preprint doi: https://doi.org/10.1101/2024.11.04.621900; this version posted November 4, 2024. The copyright holder for this preprint (which was not certified by peer review) is the author/funder, who has granted bioRxiv a license to display the preprint in perpetuity. It is made available under aCC-BY-ND 4.0 International license.

found to be elevated in 24-month-old NLFTau$^{m/h}$ mice (Fig. 1E, Table S1). Where mouse and human peptides are analogous, abundance of phosphorylation at relevant sites was analyzed in all four genotypes. However, as the standards used were for human tau, for phosphorylation sites within sequence sections that differ between the mouse and human peptides, only the genotypes containing human tau were analyzed (Fig. 1Ei, ii). The largest difference in phosphorylation was detected in the singly phosphorylated (p1) tau peptide 212-221, being significantly more abundant in NLFTau$^{m/h}$ mice than their age-matched controls (Fig. 1Eiii). Tandem mass spectrometry analysis revealed that this phosphorylation site was mostly pT217. The pT231 residue was also significantly enriched, though dependent only on the *App* mutations (Fig. 1Eiv). Notably, both these residues are typically elevated in fluid biomarkers of AD patients, compared to controls and other tauopathies[10].

Considering the increased abundance of pT217 in NLFTau$^{m/h}$, we used immunohistochemistry to investigate p-tau pathology in the soma of hippocampal CA1 pyramidal neurons, which would be indicative of initial NFT formation[9]. The pT217 tau staining appeared as two distinct morphologies: bright puncta or diffuse granular staining filling the neuronal cell body (Fig. 2A, upper panel). In order to account for both types of signals the pT217 staining was quantified as a percentage coverage within the CA1 neuronal soma (Fig. 2B).

Although some buildup of puncta and diffuse granular p-tau was evident in hippocampal neurons across all genotypes, only the 24-months NLFTau$^{m/h}$ mice showed a variable, but statistically significant, increase in pT217 soma localization, compared to levels across all genotypes at 18 months, similar to the pre-tangle morphology described in humans (Fig. 2B)[12]. Notably, at 18 months, most mice, regardless of genotype, displayed puncta of pT217. This largely remained the case for WT and Tau$^{m/h}$ mice at 24 months, with few neurons in these mice displaying the combination of p-tau puncta and diffuse granular staining that was prevalent in NLFTau$^{m/h}$ mice (Fig. 2C). Interestingly, Tau$^{m/h}$ mice exhibited significantly lower pT217 staining than WT mice at 18 months and a similar trend was observed at 24 months (Fig. 2B).

To further assess the progression of tau pathology from initial deposition in the soma to the assembly of paired helical filaments, pS396, an epitope phosphorylated within these filaments[13], was analyzed in CA1 and CA3 hippocampal neuronal cell bodies in 24-month-old NLFTau$^{m/h}$ mice compared to age-matched controls (Fig. 2A, lower panels). Although changes in the C- terminal p-tau sites were not detected in bulk tissue analysis (Fig. 1Ev-vii), spatial analysis revealed an increase in pS396 protein levels in NLFTau$^{m/h}$ mice compared to other genotypes (Fig. 2D-E). Similar to the staining observed with pT217, a small proportion of neurons in some WT, Tau$^{m/h}$ and NLF mice also showed pS396 staining in the soma, although this was greatest in NLFTau$^{m/h}$ mice in both regions (Fig. 2D-E). For pS396 staining, as the signal was more uniform, the analysis could rely on the signal intensity and was normalized to the intensity in the neighboring dendritic/axonal region. The presence of tangle-like pathology in

bioRxiv preprint doi: https://doi.org/10.1101/2024.11.04.621900; this version posted November 4, 2024. The copyright holder for this preprint (which was not certified by peer review) is the author/funder, who has granted bioRxiv a license to display the preprint in perpetuity. It is made available under aCC-BY-ND 4.0 International license.

a subset of neurons in NLFTau$^{m/h}$ mice was further confirmed by labelling with luminescent conjugated oligothiophenes (LCOs), dyes that bind to β-pleated sheets based on structural conformation (Fig. 2F).

Having established the initiation of tangle pathology in NLFTau$^{m/h}$ mice, dependent on age and the presence of Aβ plaques, we investigated whether the inclusion of human tau would also affect the deposition of plaques and p-tau levels in the immediate vicinity of these plaques, which has been consistently observed in amyloid mouse models of AD[3,14]. Plaques can be classified according to their Aβ peptide signatures and morphology, using a combination of two LCOs, q- FTAA and h-FTAA, together with an Aβ antibody, 6E10 (Fig. 3A)[15]. q-FTAA preferentially binds to mature β-pleated amyloid fibrils, whereas h-FTAA binds to both mature and immature β-pleated sheets[16]. Due to their unique emission spectrum profiles (Fig. S2A), we could distinguish between diffuse regions of Aβ or more structured plaques, thus categorizing three populations depending on their LCO positivity (Fig. 3A): 1) q-FTAA+, h-FTAA+, Aβ+ (cored plaques); 2) q-FTAA-, h-FTAA+, Aβ+ (fibrillar plaques) and 3) q-FTAA-, h-FTAA-, Aβ+ (diffuse Aβ).

At 24 months old, a significantly greater hippocampal area was occupied by diffuse Aβ compared to cored and fibrillar plaques, with no differences between NLF and NLFTau$^{m/h}$ mice (Fig. 3B, S2B). p-Tau (pS396 levels) increased with proximity to Aβ in all cases, with the greatest increase in the immediate vicinity of cored plaques. This increase was greater in NLFTau$^{m/h}$ mice than in NLF mice (Fig. 3C). The strength of pS396 staining in cored plaques positively correlated with pS396 staining in the hippocampal soma of individual NLF and NLFTau$^{m/h}$ mice, in both CA1 and CA3 regions (Fig. 3D).

Together, the above observations present a novel mouse model which addresses the major failing of previously available models. Several models have combined the two pathological hallmarks of AD, but none has achieved the initiation of NFTs triggered by Aβ accumulation, without mutations in *MAPT*. The NLF mouse has seen limited use; with more aggressive models, with rapid plaque development, receiving more attention for reasons of convenience and cost. However, age is a vital component of sporadic AD[17], making the slow time course of plaque development in this model more relevant to preclinical AD disease progression[3]. Although these plaques are caused by familial AD mutations, the humanized Aβ sequence of the NLF mouse is identical to that found in sporadic AD and the knock-in technology used avoids the overexpression-related issues typical of transgenic technology. The presence of some p-tau pathology in a subset of aged WT and Tau$^{m/h}$ mice further emphasizes the importance of ageing in modelling AD. Interestingly, an age-related increase in tau pS396 in the hippocampus of WT mice has been reported previously. In this case, the pathology was related to synaptic mitochondria, which could be a factor in age-related vulnerability[18]. Indeed it is likely that the interaction of age and Aβ pathology is vital

bioRxiv preprint doi: https://doi.org/10.1101/2024.11.04.621900; this version posted November 4, 2024. The copyright holder for this preprint (which was not certified by peer review) is the author/funder, who has granted bioRxiv a license to display the preprint in perpetuity. It is made available under aCC-BY-ND 4.0 International license.

to the unprecedented success of this model in initiating NFTs.

Moreover, in NLFTau$^{m/h}$ mice, structural maturation of Aβ deposits into cored plaques is associated with increased p-tau, reported to be related to neurotoxicity and damaged synapses[15,19]. Similarly, postmortem analysis of human brains suggests that progression to clinical dementia is associated with the prevalence of cored plaques, whereas plaques detected in cognitively normal individuals are mainly diffuse[20,21]. The positive correlation, across models, of increased p-tau pathology within cored plaques and NFT formation may suggest a causal link.

It is notable that AD, unlike most tauopathies, features NFTs containing both 4R and 3R tau at a ratio of around 60:40[22], and hence the appropriate ratio of these isoforms, achieved by expressing humanized tau heterozygously is also likely important. The only previous report of combining the two models crossed here was the *App*$^{NL\text{-}F/NL\text{-}F}$ x *MAPT* mouse, with the humanized tau expressed homozygously[6]. Although, like in other models, hyperphosphorylation of tau was reported to occur around plaques in this mouse, no reference was made to tau hyperphosphorylation in the cell soma. The 4R:3R ratio reported in this study, measured in the homozygous *MAPT* mouse, averaged around 40:60. This lower proportion of 4R tau may have impeded the development of NFTs. However, the *App*$^{NL\text{-}F/NL\text{-}F}$ x *MAPT* mouse was not the primary focus of this previous study and so the appearance of NFTs could have been missed. Thus, while it is clear that heterozygous Tau$^{m/h}$ is sufficient to initiate NFTs, whether homozygous humanized tau would also have this effect needs further investigation.

Here, we present the first mouse model in which increasing plaque load leads to delayed initiation of NFTs in old age, independent of mutations not relevant to AD. Hence, the NLFTau$^{m/h}$ mouse fulfills the 3 requirements listed above for an improved mouse model, opening future possibilities for deciphering the molecular mechanisms linking these sequential pathologies. Moreover, site-specific hyperphosphorylation of tau has been mapped in humans to show progression from diffuse granular pre-tangles to mature tangles containing β-pleated aggregates[9,12]. The similar progression in the NLFTau$^{m/h}$ mouse can now be used for testing therapies, and understanding the underlying progressive pathologies indicated by the rapid progress in availability of different plasma biomarkers[10,11].

The prevalence of AD in the human population doubles with every 5 years of age from 65 years onwards[17]. Ageing the NLFTau$^{m/h}$ mice to 30 months could reveal further disease progression. However, like humans, very old mice experience increasing mortality from different causes, necessitating large ageing colonies for reliable studies. Integrating this model with additional genetic or environmental risk factors might result in earlier-onset advanced pathologies, allowing for the study of disease progression from the beginning to end-stage. However, already the availability of a model with a clear onset of tau pathology, at an age with

bioRxiv preprint doi: https://doi.org/10.1101/2024.11.04.621900; this version posted November 4, 2024. The copyright holder for this preprint (which was not certified by peer review) is the author/funder, who has granted bioRxiv a license to display the preprint in perpetuity. It is made available under aCC-BY-ND 4.0 International license.

limited mortality rates and without mutations or overexpression of tau, is a breakthrough that opens up new possibilities for the study of AD progression. The NLFTau$^{m/h}$ mouse can now be used to guide the development of new treatments aimed at preventing or slowing clinical manifestations of the disease with every chance that findings in mice will translate to successful treatments in humans.

Funding

This study was primarily funded by grants from The Cure Alzheimer's Fund to FAE and JHardy; JHanrieder and FAE are supported by the NIH (R01 AG078796, R21AG078538, R21AG080705); Additional contributions to J.Hanrieder from the Swedish Research Council VR (#2019-02397, #2023-02796), the Swedish Alzheimer Foundation (#AF-968238, #AF-939767, #994281), Race against Dementia/Rosetree Foundation Team Award, the Swedish Brain Foundation (FO2022-0311), Åhlén-Stiftelsen. (#233011), Magnus Bergvalls Stiftelse, Stiftelsen Gamla Tjänarinnor and Gun och Bertil Stohnes Stiftelse; generous support received from the Dolby Foundation to J.Hardy; The Dementia Research Institute is funded by the Medical Research Council, UK.

bioRxiv preprint doi: https://doi.org/10.1101/2024.11.04.621900; this version posted November 4, 2024. The copyright holder for this preprint (which was not certified by peer review) is the author/funder, who has granted bioRxiv a license to display the preprint in perpetuity. It is made available under aCC-BY-ND 4.0 International license.

Methods

Animals

All experiments were carried out in accordance with the UK Animal (Scientific Procedures) Act, 1986, following local ethical review. This study used male and female *App*$^{NL\text{-}F/NL\text{-}F}$ knock-in mice, *App*$^{NL\text{-}F/NL\text{-}F}$ harboring heterozygous humanized knock-in *MAPT*, and age-matched heterozygous humanized knock-in *MAPT* and C57BL/6J wild type controls. *Mapt* knock-out mice were used as negative controls. Same sex littermates were group-housed (2-5 mice) at the UCL Biological Services Unit under a 12-hour light/dark cycle with *ad libitum* food and water supply, at a controlled temperature and humidity. Original *App*$^{NL\text{-}F/NL\text{-}F}$ and homozygous humanized knock-in *MAPT* mice were obtained from RIKEN, Japan[3,6].

Genotyping

Genotyping was performed by Transnetyx genotyping services (Cordova, TN, USA), using ear or tail tissue.

Tissue extraction

Animals were decapitated and brains were rapidly extracted on ice and hemisected. One hemisphere was drop-fixed in 10% paraformaldehyde at 4°C overnight and then stored in 30% sucrose, 0.02% sodium azide phosphate-buffered saline (PBS; 137 mM NaCl, 2.7 mM KCl, 10 mM Na_2HPO_4, 1.8 mM KH_2PO_4). The other hemisphere was dissected to extract hippocampus, cortex and cerebellum, which were snap-frozen on dry ice at –80°C for protein extraction.

Western blot

Cortical mouse brain tissue was homogenized in lysis buffer (10 mM Tris-HCl (pH 7.4), 0.8 M NaCl, 1 mM EDTA, 10% sucrose, cOmplete mini protease inhibitor cocktail (Roche #11836153001)), centrifuged at 12,000 *g* for 5 minutes at 4°C. For detection of tau isoforms, brain extracts were dephosphorylated with 0.8x $MnCl_2$ and protein metallophosphatases, and 16,000 units/ml lambda protein phosphatase at 30°C for 3 hours (New England Biolabs #P753S).

Samples were run on a 10% Bis-Tris 15-well mini 1.5 mm NuPAGE system at 160 V for 4 hours, followed by an overnight PVDF transfer at 15 V. Membranes were blocked for 1 hour at room temperature (RT) in 5% non-fat milk, 0.1% Tween 20 tris buffered saline (TBST; 20 mM Tris-HCl, 137 mM NaCl, pH = 7.6) followed by an overnight incubation at 4°C with 1:1500 anti-mouse Tau-5 antibody (Invitrogen #AHB0042) in superblock blocking buffer. The membranes were washed three times in TBST, incubated with 1:2000 horseradish peroxidase goat anti-mouse secondary antibody (Agilent #P044701-2) for 1 hour at RT in TBST with 5% (w/v) non-fat milk, washed six times in TBST and imaged using the BioRad Chemidoc imaging system. Ratio of 4R:3R peptides was quantified using Image Lab.

bioRxiv preprint doi: https://doi.org/10.1101/2024.11.04.621900; this version posted November 4, 2024. The copyright holder for this preprint (which was not certified by peer review) is the author/funder, who has granted bioRxiv a license to display the preprint in perpetuity. It is made available under aCC-BY-ND 4.0 International license.

Mass spectrometry analysis targeting tau peptides

Brain extraction, immunoprecipitation and protein digestion

Cortical brain tissue was homogenised in TBS (with cOmplete mini protease inhibitor cocktail) for 2 minutes at 200 Hz using Tissue Lyser II (Qiagen), centrifuged at 31,000 *g* for 1 hour at 4°C. Protein concentration was performed on the supernatant using the DC Protein Assay kit (Bio-Rad). The analysis of tau protein, entailing the steps of immunoprecipitation, proteolytic digestion and mass spectrometry analysis, was carried out as described previously[8]. Briefly, 20 µL of total protein from brain extracts was immunoprecipitated using 50 µL M-280 Dynabeads (Invitrogen) coated with 4 µg 77G7 anti-tau antibody (MTBR epitope 316-355, BioLegend) per sample. The antibody was chosen to bind both human and mouse tau protein. To each sample, 10 µL of tau 0N3R, 1N4R, and 2N4R isoforms standards, uniformly labelled [*U*-^{15}N], were also added. Following overnight incubation at 4°C, samples were washed, and bound proteins were subsequently eluted with 0.5% formic acid. Eluted samples were then dried in a vacuum centrifuge and stored at -80°C. Proteolytic digestion was carried out overnight at 37°C by reconstituting the samples in 50 mM ammonium bicarbonate containing 100 ng trypsin (V5111, Promega) and 100 fmol of labelled phosphorylated peptides specifically labelled at lysine [^{13}C,^{15}N-Lys] or arginine [^{13}C,^{15}N-Arg] residues, see Table S1. The next day, trypsination was stopped with the addition of 2 µL 10% formic acid. Samples were dried in a vacuum centrifuge and stored at -80°C pending mass spectrometry analysis.

Liquid chromatography-mass spectrometry

Immunoprecipitated and trypsinated samples were reconstituted in 7 µL 8% formic acid/8% acetonitrile in water and 6 µL sample solution were injected. Liquid chromatography-mass spectrometry (LC-MS) analysis was carried out using a Dionex 3000 system (Thermo Fisher Scientific) coupled to an electrospray ionization hybrid quadrupole-orbitrap mass spectrometer (Q Exactive, Thermo Fisher Scientific). LC separation was performed at a flow of 300 nL/minute using a gradient. The mass spectrometer was set to acquire in the m/z range 350–1400 in data-dependent mode using higher-energy collision-induced dissociation for ion fragmentation. Details of analysis have been previously described[8].

Processing of LC-MS data

Database searches of acquired peaks used PEAKS Studio Xpro (Bioinformatics Solutions) and Mascot Daemon v2.6.1/Mascot Distiller v2.6.3/ Mascot database search software v2.6.1 (Matrix Science). Searches were made against both UniProt and a custom-made tau-only database containing both human and mouse sequences. Quantitative analysis was performed using Skyline software v20.1.0.31 (MacCoss Lab) using the first two isotopes of the precursor ions. Search data was used to confirm the identities of peaks detected by Skyline and every peak was manually inspected. Data are shown as light-to-heavy peptide ratios. Table S1 shows the peptides included for final quantification.

bioRxiv preprint doi: https://doi.org/10.1101/2024.11.04.621900; this version posted November 4, 2024. The copyright holder for this preprint (which was not certified by peer review) is the author/funder, who has granted bioRxiv a license to display the preprint in perpetuity. It is made available under aCC-BY-ND 4.0 International license.

Immunohistochemistry

30 µm free-floating formaldehyde-fixed sections were cut transverse to the long axis of the hippocampus using a frozen sledge microtome (Leica SM2010R) and collected into PBS with 0.02% sodium azide. Sections were washed in PBS for 10 minutes, followed by antigen retrieval in 10 mM sodium citrate buffer (pH 9.0) at 80°C for 30 minutes. Tissues were permeabilized in three 10-minute 0.3% Triton-X 100 PBS (PBST) washes and then incubated in blocking buffer (3% normal goat, 0.3% PBST) for 1 hour at RT. The sections were subsequently incubated overnight at 4°C with appropriate primary antibodies in blocking buffer; 1:1000 rabbit anti- phosphotau-threonine217 (pT217, Invitrogen, #44-744), 1:000 rabbit anti-phosphotau-serine396, (pS396, Invitrogen, #44-752G), 1:500 mouse anti-amyloid, 1-16 (6E10, Biolegend, #803004).

The next day, sections were washed three times in 0.3% PBST for 10 minutes each, followed by a 2-hour incubation with appropriate secondary antibodies in blocking buffer in the dark at RT; 1:000 goat anti-rabbit Alexa Flour 647 (Invitrogen, # A21244), 1:1000 goat anti-mouse Alexa Flour 594 (Invitrogen, #A11032). Subject to three 10-minute 0.3% PBST washes, sections were incubated with a combination of two luminescent conjugated oligothiophenes (LCOs, 1:500 tetrameric and 1:1500 heptameric formic thiophene acetic acid; q-FTAA and h-FTAA, respectively) in the dark at RT for 30 minutes. Finally, nuclei were counterstained with 4′,6-diamidino-2-phenylindole (DAPI) for 5 minutes at RT.

Fluorescent Imaging

All imaging was performed on the Zeiss LSM 880 confocal microscope with a 32-channel GaAsP spectral detector. For LCO analysis, q- and h-FTAA dyes were excited by a 458 nm argon laser. Using reference emission spectra of the two dyes obtained by hyperspectral imaging in lambda mode, linear unmixing was subsequently performed to obtain separate images for q- and h-FTAA in the multi-stained samples, as described previously[15].

Confocal photomicrographs of hippocampal tissue, multi-stained with q-FTAA and h-FTAA, were acquired as z-stack images (3-µm intervals) using a Plan-Apochromat 20× objective (NA 0.8).

Additionally, the same samples were stained with DAPI, pS396, and 6E10, and imaged as widefield photomicrographs using the same objective. These images were then merged into a single file for comprehensive analysis. pT217 and DAPI were imaged with a Plan-Apochromat 40× objective oil (0.8 NA) under constant laser power, master and digital gain, and offset settings.

bioRxiv preprint doi: https://doi.org/10.1101/2024.11.04.621900; this version posted November 4, 2024. The copyright holder for this preprint (which was not certified by peer review) is the author/funder, who has granted bioRxiv a license to display the preprint in perpetuity. It is made available under aCC-BY-ND 4.0 International license.

Immunohistochemical analysis

Immunohistochemical staining analyses were performed using custom-made semi-automated macros on ImageJ (as described below):

Plaque load analysis

The hippocampal region for each image was manually selected and thresholded to adjust for individual background differences, as previously described[23]. Particles less than 10 μm^2 were excluded from analysis. Plaques were subsequently classified as either q-FTAA+, h-FTAA+, Aβ+ (cored plaques) or q-FTAA-, h-FTAA+, Aβ+ (fibrillar plaques).

Protein analysis around plaques

For each cored and fibrillar plaque identified within the selected hippocampal region of interest (ROI), concentric contours preserving the original shape of each plaque were drawn outwards with increasing radial increments (radii from plaque edge (μm); 0, 5, 10, 20, 30; fig.3). Where concentric contours of cored and fibrillar plaques overlapped, the ROI in this overlapping region was omitted from further analysis. It is noteworthy that while all LCO+ plaques are also positive for Aβ, not all Aβ staining is positive for LCO. To exclusively analyze the spatial effect of Aβ on protein intensity, concentric contours, as described above, were drawn for Aβ+ LCO- regions. ROIs with overlapping contours between Aβ+ and LCO+ plaques were excluded from further analysis. Subsequently, protein florescence intensity within plaque and radiating regions was calculated as a fold-change compared to 30 μm from the respective plaque type.

Protein analysis within hippocampal pyramidal cells

In the hippocampal CA1 and CA3 pyramidal cell layer, concentric contours were drawn around each identified DAPI nucleus to maintain its original shape, extending 3.5 μm away from the DAPI edge to delineate cytoplasmic regions as ROIs. Any overlapping regions were merged as a single larger ROI. Protein florescence intensity within these ROIs was calculated as fold-change from mean protein florescence intensity in the dendritic region. To identify the percentage coverage of protein within the identified cytoplasmic ROIs, the top 5% of pixels in each image were selected based on a histogram of pixel intensity distribution and used as the threshold for real signal.

Statistical Analysis

Analysis was performed using GraphPad Prism 10 or SPSS as indicated. Samples sizes represent number of animals and any technical replicates obtained from a single animal were averaged for that animal. Analysis of variance or generalized linear mixed model was applied as appropriate, dependent on the number of variables compared.

bioRxiv preprint doi: https://doi.org/10.1101/2024.11.04.621900; this version posted November 4, 2024. The copyright holder for this preprint (which was not certified by peer review) is the author/funder, who has granted bioRxiv a license to display the preprint in perpetuity. It is made available under aCC-BY-ND 4.0 International license.

References

1 Long, J. M. & Holtzman, D. M. Alzheimer Disease: An Update on Pathobiology and Treatment Strategies. *Cell* **179**, 312-339 (2019). https://doi.org/10.1016/j.cell.2019.09.001

2 Oddo, S. *et al.* Triple-transgenic model of Alzheimer's disease with plaques and tangles: intracellular Abeta and synaptic dysfunction. *Neuron* **39**, 409-421 (2003).

3 Saito, T. *et al.* Single App knock-in mouse models of Alzheimer's disease. *Nat Neurosci* **17**, 661-663 (2014). https://doi.org/10.1038/nn.3697

4 Benitez, D. P. *et al.* Knock-in models related to Alzheimer's disease: synaptic transmission, plaques and the role of microglia. *Mol Neurodegener* **16**, 47 (2021). https://doi.org/10.1186/s13024-021-00457-0

5 Goedert, M., Spillantini, M. G., Jakes, R., Rutherford, D. & Crowther, R. A. Multiple isoforms of human microtubule-associated protein tau: sequences and localization in neurofibrillary tangles of Alzheimer's disease. *Neuron* **3**, 519-526 (1989).

6 Saito, T. *et al.* Humanization of the entire murine Mapt gene provides a murine model of pathological human tau propagation. *J Biol Chem* **294**, 12754-12765 (2019). https://doi.org/10.1074/jbc.RA119.009487

7 Takuma, H., Arawaka, S., Mori, H. Isoforms changes of tau protein during development in various species. *Dev Brain Res* **142**, 121-127 (2003).

8 Lantero-Rodriguez, J. *et al.* Tau protein profiling in tauopathies: a human brain study. *Mol Neurodegener* **19**, 54 (2024). https://doi.org/10.1186/s13024-024-00741-9

9 Moloney, C. M. *et al.* Phosphorylated tau sites that are elevated in Alzheimer's disease fluid biomarkers are visualized in early neurofibrillary tangle maturity levels in the post mortem brain. *Alzheimers Dement* (2022). https://doi.org/10.1002/alz.12749

10 Mila-Aloma, M. *et al.* Plasma p-tau231 and p-tau217 as state markers of amyloid-beta pathology in preclinical Alzheimer's disease. *Nat Med* **28**, 1797-1801 (2022). https://doi.org/10.1038/s41591-022-01925-w

11 Ankeny, S. E., Bacci, J. R., Decourt, B., Sabbagh, M. N. & Mielke, M. M. Navigating the Landscape of Plasma Biomarkers in Alzheimer's Disease: Focus on Past, Present, and Future Clinical Applications. *Neurol Ther* (2024). https://doi.org/10.1007/s40120-024- 00658-x

12 Moloney, C. M., Lowe, V. J. & Murray, M. E. Visualization of neurofibrillary tangle maturity in Alzheimer's disease: A clinicopathologic perspective for biomarker research. *Alzheimers Dement* **17**, 1554-1574 (2021). https://doi.org/10.1002/alz.12321

13 Otvos, L., Jr. *et al.* Monoclonal antibody PHF-1 recognizes tau protein phosphorylated at serine residues 396 and 404. *J Neurosci Res* **39**, 669-673 (1994). https://doi.org/10.1002/jnr.490390607

14 Forner, S. *et al.* Systematic phenotyping and characterization of the 5xFAD mouse model of Alzheimer's disease. *Sci Data* **8**, 270 (2021). https://doi.org/10.1038/s41597-021- 01054-y

15 Wood, J. I. *et al.* Isotope Encoded chemical Imaging Identifies Amyloid Plaque Age

bioRxiv preprint doi: https://doi.org/10.1101/2024.11.04.621900; this version posted November 4, 2024. The copyright holder for this preprint (which was not certified by peer review) is the author/funder, who has granted bioRxiv a license to display the preprint in perpetuity. It is made available under aCC-BY-ND 4.0 International license.

Dependent Structural Maturation, Synaptic Loss, and Increased Toxicity. *bioRxiv* (2024). https://doi.org/10.1101/2024.10.08.617019

16 Nystrom, S., Back, M., Nilsson, K. P. R. & Hammarstrom, P. Imaging Amyloid Tissues Stained with Luminescent Conjugated Oligothiophenes by Hyperspectral Confocal Microscopy and Fluorescence Lifetime Imaging. *J Vis Exp* (2017). https://doi.org/10.3791/56279

17 Brookmeyer, R., Gray, S. & Kawas, C. Projections of Alzheimer's disease in the United States and the public health impact of delaying disease onset. *Am J Public Health* **88**, 1337-1342 (1998). https://doi.org/10.2105/ajph.88.9.1337

18 Torres, A. K., Jara, C., Olesen, M. A. & Tapia-Rojas, C. Pathologically phosphorylated tau at S396/404 (PHF-1) is accumulated inside of hippocampal synaptic mitochondria of aged Wild-type mice. *Sci Rep* **11**, 4448 (2021). https://doi.org/10.1038/s41598-021-83910-w

19 Koutarapu, S. *et al.* Chemical signatures delineate heterogeneous amyloid plaque populations across the Alzheimer's disease spectrum. *bioRxiv* (2024). https://doi.org/10.1101/2024.06.03.596890

20 Malek-Ahmadi, M., Perez, S. E., Chen, K. & Mufson, E. J. Neuritic and Diffuse Plaque Associations with Memory in Non-Cognitively Impaired Elderly. *J Alzheimers Dis* **53**, 1641-1652 (2016). https://doi.org/10.3233/JAD-160365

21 Dickson, D. W. *et al.* Identification of normal and pathological aging in prospectively studied nondemented elderly humans. *Neurobiology of Aging* **13**, 179-189 (1992). https://doi.org/https://doi.org/10.1016/0197-4580(92)90027-U

22 Dregni, A. J. *et al.* Fluent molecular mixing of Tau isoforms in Alzheimer's disease neurofibrillary tangles. *Nat Commun* **13**, 2967 (2022). https://doi.org/10.1038/s41467-022-30585-0

23 Wood, J. I. *et al.* Plaque contact and unimpaired Trem2 is required for the microglial response to amyloid pathology. *Cell Rep* **41**, 111686 (2022). https://doi.org/10.1016/j.celrep.2022.111686

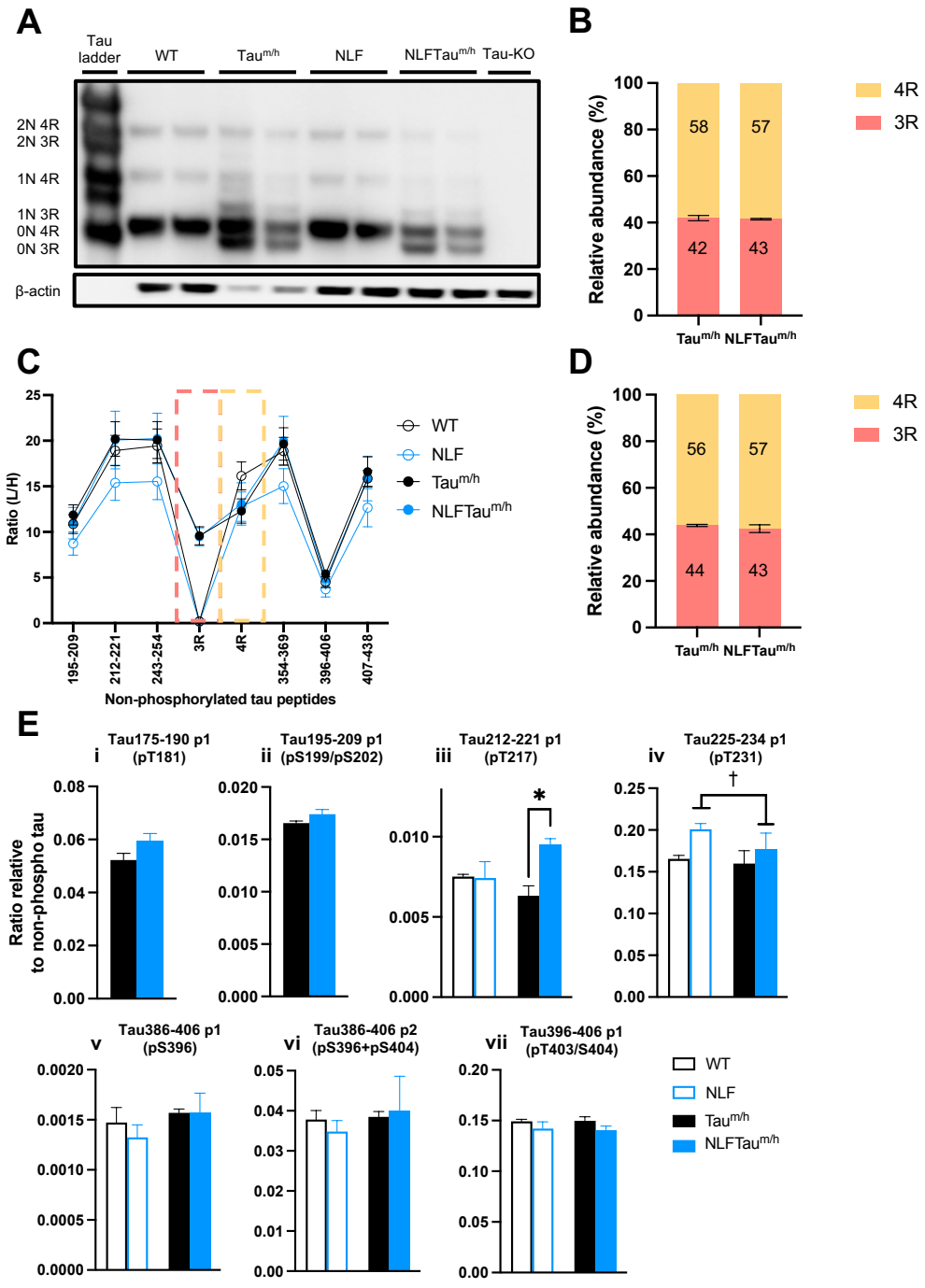

Figure 1. Analysis of tau peptides in WT, NLF, Tau$^{m/h}$ and NLFTau$^{m/h}$ mice.
(A) Immunoblotting of total tau detected by Tau-5. β-actin is used as a loading control. **(B)** Relative quantification of 3R and 4R tau isoforms from **(A)** (Tau$^{m/h}$ n = 4, NLFTau$^{m/h}$ n = 3 mice). **(C)** Quantification of non-phosphorylated tau peptides by IP-MS analysis (Two-way ANOVA; WT n = 4, NLF n = 5, Tau$^{m/h}$ n = 4, NLFTau$^{m/h}$ n = 3 mice). **(D)** Relative abundance of 3R and 4R tau isoforms from **(C)**. **(E)** Abundance of tau peptides carrying one (p1) or two (p2) phosphorylations, relative to non-phosphorylated 354-369 tau peptide level by IP-MS analysis (Two-way ANOVA; WT n = 4, NLF n = 5, Tau$^{m/h}$ n = 4, NLFTau$^{m/h}$ n = 3 mice). *Post hoc* Sidak's multiple comparisons test shown as *p<0.05, main effect of *App* mutations shown as †p<0.05. Data in **B-E** is represented as mean ± SEM.

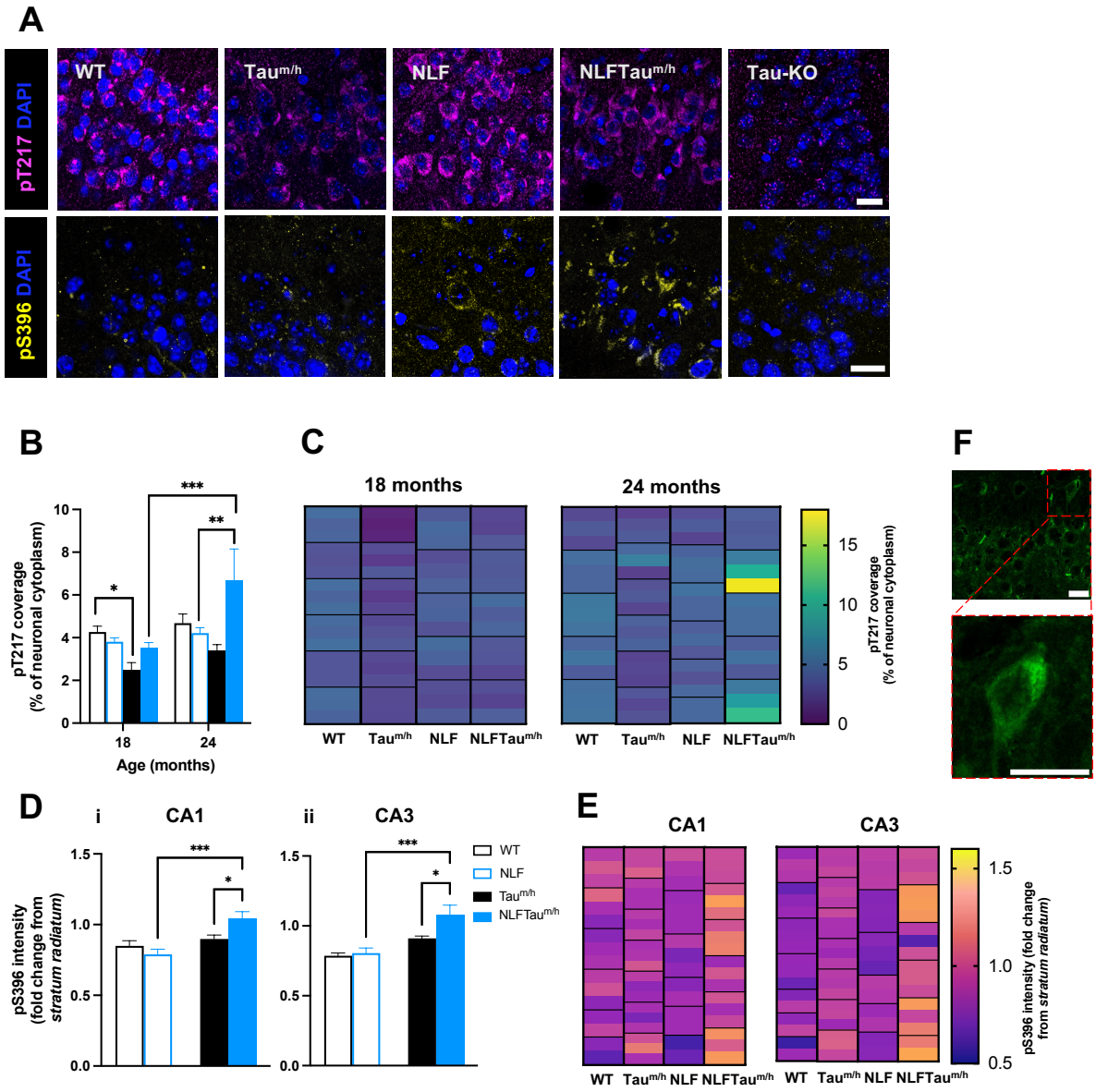

Figure 2. Changes in p-tau levels across age and genotype in hippocampal neurons. **(A)** Representative images of pT217 and pS396 staining across genotypes in CA1 hippocampal neurons. Scale bar: 20μm for all panels. **(B)** pT217 coverage within neuronal cytoplasm across age and genotype. Generalized linear mixed model analysis followed by a least significant difference *post hoc* analysis. ***p<0.001, **p<0.01, *p<0.05. **(C)** Heatmaps showing distribution of pT217 coverage across genotypes at 18 and 24 months. Each black outlined box represents a biological replicate, while the boxes within indicate technical replicates. **(D)** pS396 florescence intensity in CA1 and CA3 hippocampal pyramidal neurons as a fold-change from pS396 florescence intensity in the *stratum radiatum.* Two-way ANOVA *post hoc* Sidak's multiple comparisons are shown on the graphs. ***p<0.001, **p<0.01, *p<0.05. **(E)** Heatmaps show the distribution of pS396 florescence intensity across genotypes in CA1 and CA3 hippocampal pyramidal neurons. Each black outlined box represents a biological replicate, while the boxes within indicate technical replicates. **(F)** LCO staining in the NLFTau$^{m/h}$ mouse indicates β-pleated sheet structures in a subset of hippocampal neurons. Lower panel: high-resolution scan of neuron shown in upper panel. Scale bar: 20μm for both panels. Data in **B, D** are presented as mean ± SEM.

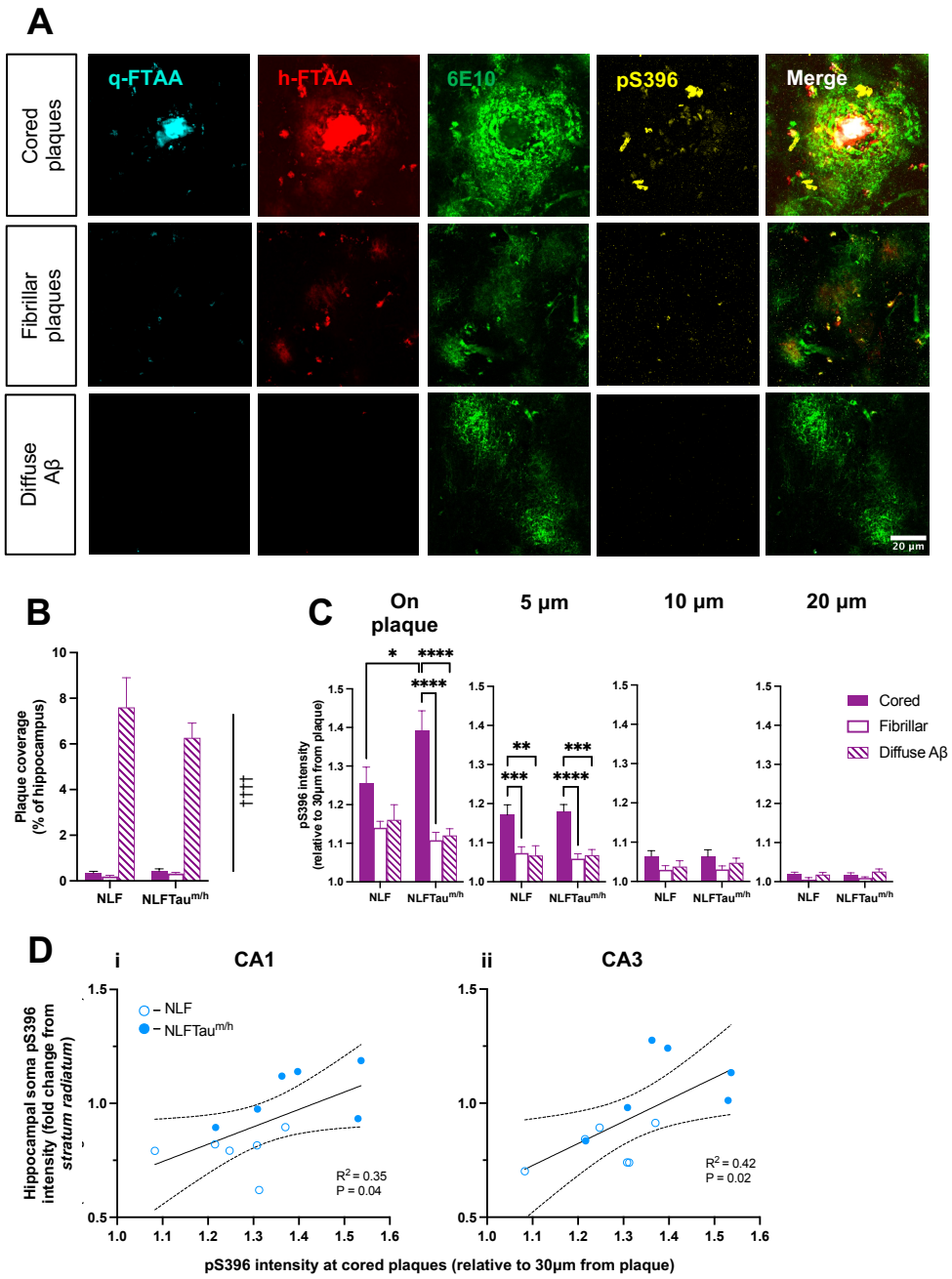

Figure 3. P-tau levels around cored and fibrillar plaques and diffuse Aβ.
(A) Representative images of different plaque types and associated pS396 protein levels. Scale bar at the bottom right: 20 µm for all panels **(B)** Hippocampal coverage of different plaque types in 24-month-old NLF and NLFTau$^{m/h}$ mice. Two-way ANOVA: main effect of plaque type is shown as ††††p<0.0001. **(C)** pS396 tau fluorescence intensity on the plaque, 5, 10, 20 µm from the edge of respective plaque types expressed as a fold change relative to 30 µm in 24-month-old NLF and NLFTau$^{m/h}$ mice. Generalized linear mixed model analysis followed by a sequential Sidak *post hoc* analysis. *p<0.05; **p<0.01; ***p<0.001; ****p<0.0001. Data in **B,C** are presented as mean ± SEM. NLF N = 6 mice; NLFTau$^{m/h}$ N = 6 mice (2-3 technical replicates per mouse). **(D)** Correlation of pS396 intensity within the CA1 **(i)** and CA3 **(ii)** neuronal soma versus pS396 intensity at cored plaques. Lines represent linear regression with 95% confidence intervals.

Figure S1. Comparison of human and mouse 2N4R tau protein isoform sequence. Amino acids highlighted in dark blue are identical between human and mouse tau, while light blue indicate differences. Dashed lines show regions where amino acids are missing in one of the sequences. Numbers along the sides serve as reference points for amino acid positions. Sequence alignment was made using Jalview.

Measured peptide	Phosphorylation site	Peptide Sequence
195-209	NA	SGYSSPGSPGTPGSR
212-221	NA	TPSLPTPPTR
243-254	NA	LQTAPVPMPDLK
275-286 (3R)	NA	VQIVYKPVDLSK
299-317 (4R)	NA	HVPGGGSVQIVYKPVDLSK
354-369	NA	IGSLDNITHVPGGGNK
396-406	NA	SPVVSGDTSPR
407-438	NA	HLSNVSSTGSIDMVDSPQLATLADEVSASLAK
175-190 p1	T181	TPPAPK**T**PPSSGEPPK
195-209 p1	S199	SGYS**S**PGSPGTPGSR
	S202	SGYSSPG**S**PGTPGSR
212-221 p1	T217	TPSLP**T**PPTR
225-234 p1	T231	KVAVVR**T**PPK
386-406 p1	S396	TDHGAEIVYK**S**PVVSGDTSPR
386-406 p2	S396 + S404	TDHGAEIVYK**S**PVVSGDT**S**PR
396-406 p1	T403	SPVVSGD**T**SPR
	S404	SPVVSGDT**S**PR

Table S1. Quantified tau peptides: phosphorylated and non-phosphorylated.
Phosphorylation sites within specific peptide sequences are shown in bold. Phosphorylated peptide standards were labelled at lysine [$^{13}C_6$,$^{15}N_2$-Lys] or arginine [$^{13}C_6$,$^{15}N_2$-Arg] residues. All non-phosphorylated peptide standards were uniformly labelled with [*U*-^{15}N].

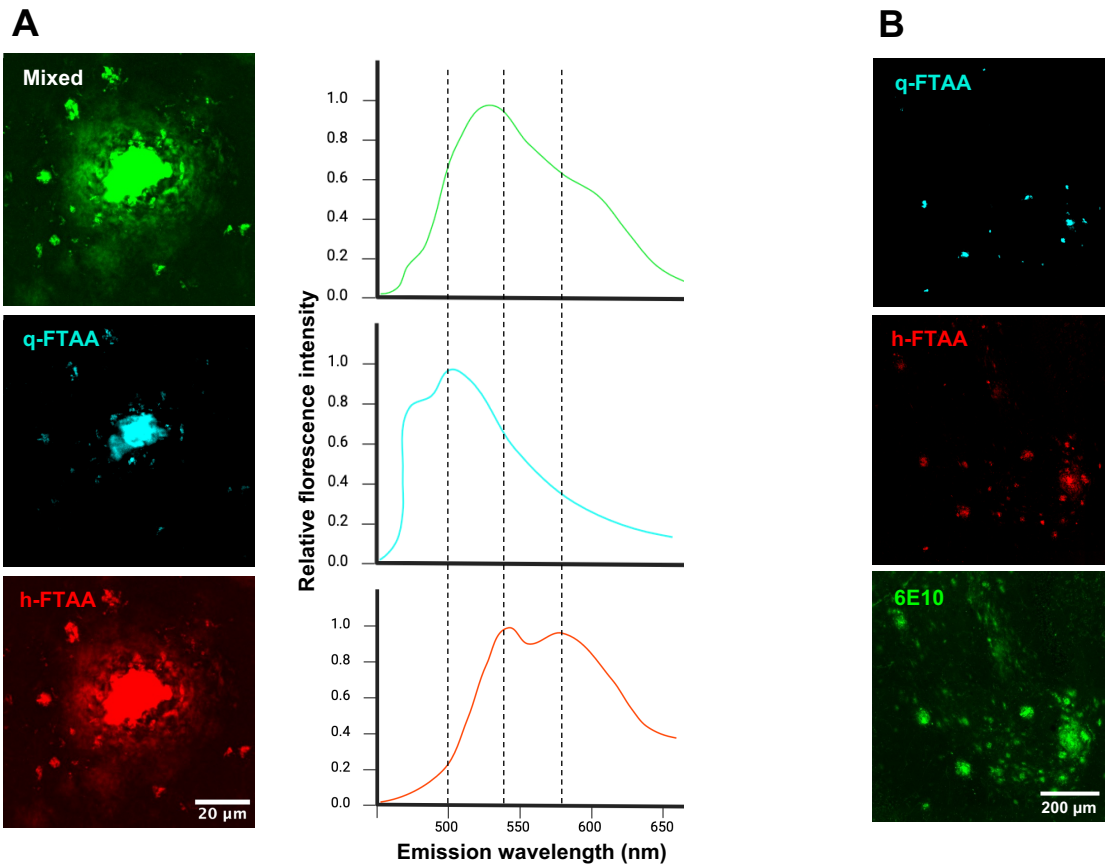

Figure S2. Plaques can be classified according to their amyloid content using conformation-sensitive LCOs.
(A) Each LCO exhibits a distinct spectral emission profile, identifiable with a hyperspectral detector in lambda mode (405 – 750 nm) for each pixel when stimulated at 458 nm. q-FTAA shows a blue-shifted peak at 500 nm, while h-FTAA displays red-shifted peaks between 540 and 580 nm. Linear unmixing allows for the separation of mixed LCO signals into distinct q-FTAA and h-FTAA channels. **(B)** An overview of q-FTAA, h-FTAA and 6E10 Aβ staining distribution in the hippocampus.